ISSN 1547-4771, Physics of Particles and Nuclei Letters, 2015, Vol. 12, No. 2, pp. 336–343. © Pleiades Publishing, Ltd., 2015.
Original Russian Text © E.P. Shabalin, A.E. Verkhoglyadov, M.V. Bulavin, A.D. Rogov, E.N. Kulagin, S.A. Kulikov, 2015, published in Pis'ma v Zhurnal Fizika Elementarnykh Chastits i Atomnogo Yadra, 2015.

METHODS OF PHYSICAL EXPERIMENT

Spectrum and Density of Neutron Flux in the Irradiation Beam Line No. 3 of the IBR-2 Reactor

E. P. Shabalin, A. E. Verkhoglyadov, M. V. Bulavin, A. D. Rogov, E. N. Kulagin, and S. A. Kulikov

Joint Institute for Nuclear Research, Dubna, Russia

e-mail: verhoglyadov_al@mail.ru

Abstract—Methodology and results of measuring the differential density of the neutron flux in irradiation beam line no. 3 of the IBR-2 reactor using neutron activation analysis (NAA) are presented in the paper. The results are compared to the calculation performed on the basis of the 3D MCNP model. The data that are obtained are required to determine the integrated radiation dose of the studied samples at various distances from the reactor.

DOI: 10.1134/S154747711502020X

1. SAMPLES AND IRRADIATION CONDITIONS FOR NEUTRON-FLUX MEASUREMENTS

Energy spectrum and neutron-flux densities were measured using neutron activation analysis (NAA) (see, for example, [1]). Samples to be irradiated were placed on the supporting transport beam of the irradiation facility at distances of 300, 500, and 3150 mm from the water-moderator surface of the IBR-2 reactor within the direct visibility of the reactor. In addition, the induced activity of Ni was measured along the whole length of the supporting beam. Samples were irradiated at a reactor power of 1.85–1.9 MW for 56 h of the effective irradiation time on April 18–20, 2013, and for 178 h on October 14–22, 2013. The additional irradiation of indium and tin samples was performed at 440 kW for 3 h.

Samples for an NAA measurement of the neutron-flux during the reactor session on April 2013 were grouped into two clusters, specifically the near and the far ones. In the process of irradiation, the near cluster was placed at a distance of 500 mm from the surface of the water moderator of neutrons in the reactor and the far cluster was placed at a distance of 3150 mm; both clusters were oriented in a parallel manner to the moderator surface.

Certified samples with a purity of 99.56–99.99% from sample collections no. 1551 (Al, Cu, Fe, and In) and no. 1552 (Co, Mo, NaCl, and W) produced by Thermo Electron Corporation were used in irradiation experiments. In addition, high-purity foils of vanadium, titanium, and gold (ultrathin foil with thickness of 1 μm) were used, as was nickel foil with a molybdenum content of about 20%, nichrome and tin-lead alloys (with 80% of Ni and 91% of tin, respectively), and cobalt in the form of sodium cobaltate salt.

The sample mass varied from 10 mg (gold) to several grams (aluminum at a large distance from the

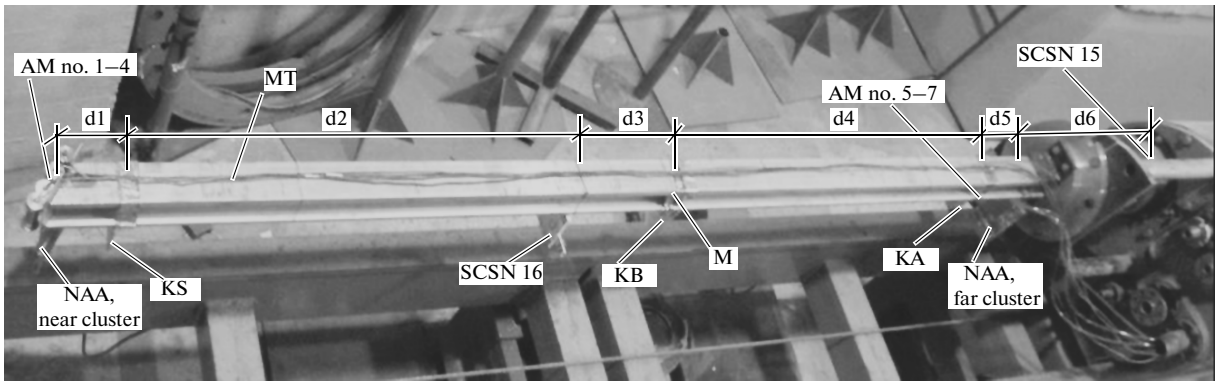

Fig. 1. Image of the transport beam with samples for NAA and nichrome wire for an estimation of neutron-flux behavior along the beam.

Fig. 2. Image of studied samples in the package (cadmium, aluminum, or copper).

Fig. 3. Image of the germanium detector.

reactor and vanadium), depending on the neutron flux and neutron cross section in the measured energy range. Part of the isotopes was irradiated with and without cadmium shield.

A total of 14 isotopes in 42 samples were irradiated. A dedicated processing technique was used; it turned out that ten isotopes (eight elements), specifically V, Al, Ti (3 isotopes), Ni, Sn, Au, Co, and Na, were sufficient for reconstructing the energy spectrum and neutron-flux density.

2. SAMPLE ACTIVITY MEASUREMENT TECHNIQUE

The activity of the irradiated samples was measured using IGC 21 germanium detector (Princeton Gamma-Tech) with TsSU-V-1K digital spectrometer and GammaMCA-8000 software (Fig. 3). The detector chamber was located far from radiation sources (reactor and NAA samples) and had no windows. Hence, a low background level was ensured during measurements, even with no additional lead shield for the detector crystal. Only one measured sample at a time was placed at the detector chamber.

To reduce the workload of the detection system, part of samples were placed at a certain height above the detector surface using a pedestal.

To determine the absolute efficiency of the detection system, measurements were performed using a set of reference radiation sources for gamma ray spectrometry; as a result, we obtained

(i) absolute efficiency as a function of quantum energy E and sample height above the detector; in Fig. 4, the dependence of efficiency on energy is presented for the height of 100 mm;

(ii) absolute efficiency corrections due to geometric sizes of the samples (for the samples measured at the detector surface);

(iii) limit workloads of the system, above which spectral and dead-time distortions are observed.

The sample height above the detector was selected in a way that dead time would not exceed 4%, which corresponds to a workload of 1000–1200 pulses per second. As statistical data are collected, the peak of the desired isotope is determined in the spectrum and the quantity of pulses at this peak, as well as statistical error, are calculated (GammaMCA software performs the calculations during the measurement). When the error in determining the peak area reaches the required value (typically less than 1%), the measurement stops and the spectrum is saved in a file.

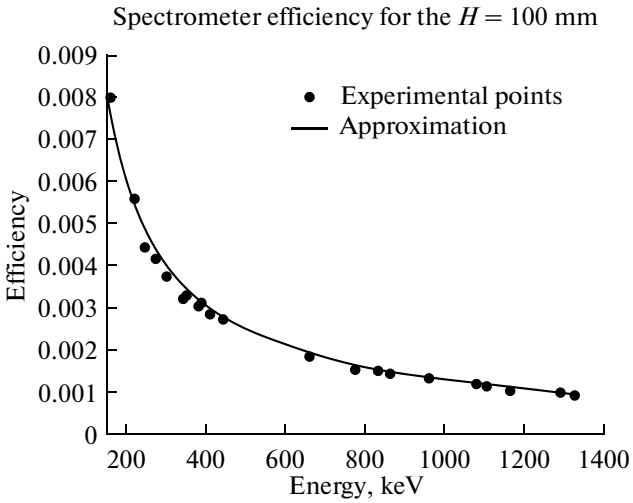

Fig. 4. Dependence of the detector efficiency on energy for the height $h = 100$ mm.

The transition from the activity of the irradiated sample during the measurement at the detector to isotope activity during the continuous long-term irradiation per atom considering the time dependence of the reactor power during irradiation (i.e., the integral of the product of reaction cross section and neutron-flux density) was carried out using the well-known formulas [1]. The half-life of the isotope $T_{1/2}$ and gamma quantum yield I_g were taken from the library http://nucleardata.nuclear.lu.se/toi/radSearch.asp.

3. SPECTRUM RECONSTRUCTION PROCEDURE AND THE RESULTS

The procedure relied on the assumption of the presence of five neutron energy regions, each of which have an energy dependence of the differential neutron-flux density described by an individual function. The rationale behind this assumption is as follows.

First, three regions are clearly defined based on fundamental properties of neutron moderation and diffusion. These are thermal or subcadmium neutrons (with energies below 0.5 eV), slowing-down neutrons with energies of 0.5 eV to ~0.1 MeV, and fast neutrons. Thermal neutrons (thermalized in water of the external moderator) are distributed under the Maxwell law up to energies of about 0.2 eV. The energy distribution of slowing-down neutrons has an exponential nature; in the case of graphite or heavy water moderators, the differential flux density is inverse proportional to the neutron energy and, in the case of light water moderators, it is described by the function

$$\Phi(E) = C_x E^{-\beta_x}, \quad (1)$$

where exponent value β_x is less than 1.

Second, according to the known set of threshold isotopes, the fast neutron region with $E > 0.1$ MeV may be divided into three subregions: 0.1–1 MeV, 1–5 MeV, and 5–14 MeV.

Finally, it is known that the differential neutron-flux density in systems with a hydrogen moderator decreases monotonically with energy throughout the whole energy range, apart from the thermalized region. This is further confirmed by the shape of the neutron spectrum calculated for the IBR-2 with actual reactor geometry and environment using MCNP-X5 software [2]. Reconstructed and calculated spectra will be compared in the corresponding section of the paper below.

The principle of dividing the whole neutron energy range into five groups and assumption of monotonicity of the functions made it possible to reconstruct the shape of functions of differential neutron-flux density *analytically* without resorting to complicated methods for solving ambiguous inverse problems. To achieve this, an independent approximation of differential energy density of the neutron flux with *monotonous trial functions with two parameters* was applied to all groups of the energy spectrum specified above. The final choice of the shape and parameters of the function from the set of analytically obtained data was performed based on the generally accepeted criterion, according to which the total mean-square deviation of the measured and calculated sample activities is to be minimized.

Let us consider the spectrum reconstruction procedure based on sample activity data at each energy region individually.

$E > 5$ MeV

This part of the neutron energy spectrum was reconstructed using reactions that only have nonzero cross sections in the given region: $Al^{27}(n, \alpha)Na^{24}$, $V^{51}(n,\alpha)Sc^{48}$, $Cu^{63}(n, \alpha)Co^{60}$, and $Ti^{48}(n, p)Sc^{48}$. Functions with two parameters written as

$$\Phi(E) = C_1 \cdot e^{-\alpha_1 E}, \quad (2.1)$$

$$\Phi(E) = C_2 \cdot \frac{e^{-\alpha_2 E}}{E}, \quad (2.2)$$

and the power function similar to (1) were tested as trial functions.

The use of functions with two parameters simplifies the solution of the inverse problem. For instance, it makes it possible to reduce the minimization of the functional

$$\chi^2 = \sum_{i=1}^{k} \left(\frac{A_{\text{exp},i} - A_{\text{cal},i}}{A_{\text{exp},i}} \right)^2 \quad (3)$$

to obtain the roots of linear and transcendental equations.

In (3), $A_{\text{exp},i} = \int_0^\infty \sigma_i(E)\Phi(E)dE$ is the experimental activity value of isotope i rescaled for infinite continuous irradiation time and one atom, and $A_{\text{cal},i}$ is the same value calculated for thetrial function $\Phi_x(E)$.

The procedure of obtaining a χ^2 minimum for each trial function was as follows:

1. Function $C_x(\alpha)$ was calculated (where C_x is the normalization coefficient for the neutron flux, see (2)) based on the χ^2 minimum for α values within the wide interval selected. It can be easily seen that the problem here was to calculate the integrals $\int_0^\infty \sigma_i(E)\frac{\Phi_x(E)}{C_x}dE$ and subsequently solve the linear equation.

2. Then, the α_x parameter was determined based on χ^2 minimum using the previously calculated function $C_x(\alpha)$ in (3). The transcendental equation had to be solved for this purpose.

The final choice between three approximation functions for the neutron flux (see (2)) corresponded to the minimuum χ^2 value.

Among the three trial functions, the minimum value $\chi^2 = 0.0015$ was demonstrated by the power function (2.1) with parameters $C_1 = 0.47 \times 10^{12}$ n cm^{-2} s^{-1} MeV^{-1} and $\alpha = 0.693$ MeV^{-1}. The standard deviation of the reconstructed neutron flux from the true one under the fixed α does not exceed 4%. Taking into account the presence of neutron-flux gradients of about 2% per centimeter at the sample placement area, the error of the coefficient C_1 is to be further increased by ±4%, thereby leading to

$$C_1 = (0.47 \pm 0.04) \times 10^{12} \text{ n cm}^{-2} \text{ s}^{-1} \text{ MeV}^{-1}.$$

For the sake of clarity and elaboration, functions $C(\alpha) = \dfrac{A_{\exp,i}}{\int_0^\infty \sigma_i(E)\Phi_x(E)dE}$ are presented for several isotopes in Fig. 5; parameter C is measured in n cm^{-2} s^{-1} MeV^{-1}.

Function (2.2) also provided a small χ^2 value, specifically, $\chi^2 = 0.027$, for parameter values $\alpha = 0.7$ MeV^{-1} and $C = 1.79 \times 10^{12}$ n cm^{-2} s^{-1} MeV^{-1} (in the case of neutron flux at the distance of 0.3 m from the reactor). Functions (2.1) and (2.2) differ in the region of $E > 7$ MeV by, at most, 3%. However, the use of exponential function is more convenient for blending with the neutron-flux function for energies below 5 MeV (see below). In addition, it can be integrated analytically, which is convenient in terms of application.

The differential energy density of the neutron flux at the distance of 0.5 m from the reactor moderator reconstructed using the NAA in the region with neutron energies above 5 MeV may also be expressed by the exponential function

$$\Phi(E) = (0.216 \pm 0.02)e^{-0.693E} \times 10^{12} \text{ n cm}^{-2} \text{ s}^{-1} \text{ MeV}^{-1}.$$

Region of 1–5 MeV

Isotopes Ti^{46}, Ti^{47}, Fe^{54}, and Ni^{58} for the group of threshold indicators with reaction threshold (n, p) within the range of 1–3 MeV. Two isotopes In^{115} and Sn^{117} with low reaction thresholds of 0.3–0.4 MeV, which form radioactive isomers under the inelastic scattering of fast neutrons, should also be attributed to this group, because effective thresholds for these reactions turn out to be close to 1 MeV in the case of the measured spectrum.

It is worth noting that natural tin is barely used in NAA, since significant amounts of the same isomer Sn-117m are produced as a result of resonance neutron capture by the Sn-116 isotope. However, in the present paper, natural tin was successfully used for activation (during irradiation session at the distance of 0.3 m), with resonance neutron capture by Sn-116 ($E_{res} = 112$ eV) prevented using the boron filter enriched with boron-10 up to 80%.

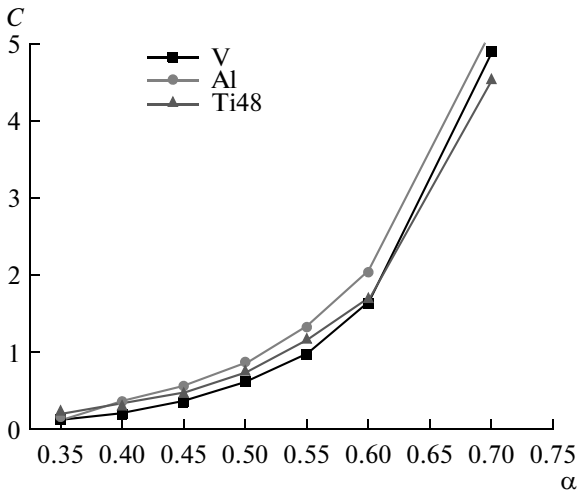

Fig. 5. Dependence of coefficient C on parameter α (measured in 10^{12} n cm^{-2} s^{-1} MeV^{-1}) for function (2.1).

To perform spectrum reconstruction in the region of 1–5 MeV, the previously obtained result for the region with $E > 5$ MeV was used with the addition of the $C_2\dfrac{e^{-\alpha E}}{E}$ function. Parameters of the function were determined using the method described above. Thus, differential energy density of the neutron flux for distances of 0.3 and 0.5 m in the energy region of 1–5 MeV may be described rather well by the function

$$\Phi(E) = \left(C_1 \cdot e^{-0.693E} + C_2 \cdot \frac{e^{-\alpha E}}{E}\right) \times 10^{12} \text{ n cm}^{-2} \text{ s}^{-1} \text{ MeV}^{-1}, \quad (4)$$

where $\alpha \approx 1$ and values of C coefficients are presented in Table 1 below. The error of the coefficient C_2 is about ±5%.

The Region of 0.1–1 MeV

Unfortunately, estimating neutron flux in this energy region using NAA turned out to be impossible due to absence of suitable threshold indicators for the experiment. To cover this region, X-ray and beta spec-

Table 1. Coefficient values in formulas (4) and (7), which describe the differential energy density of the neutron flux in beam line no. 3 of the IBR-2 reactor

L, m	C_1	C_2
0.3	0.47	0.39
0.5	0.216	0.183
0.7	0.085	0.072

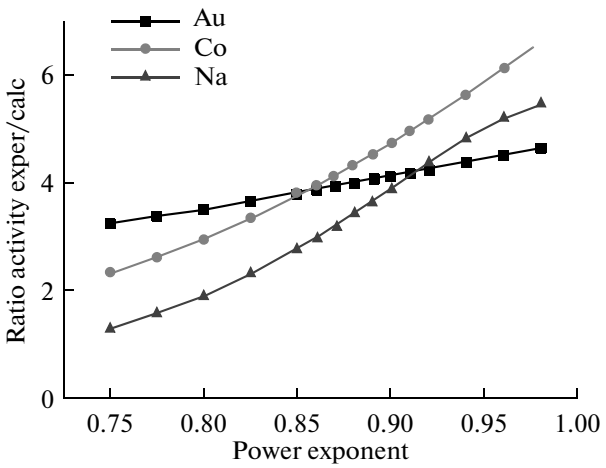

Fig. 6. Dependence of the C oefficient (measured in 10^{11} n cm^{-2} s^{-1} MeV^{-1}) in function (1) on the parameter α.

trometers, as well as short-lived isotopes, should be used.

Resonance Region

The isotopes used for spectrum reconstruction in the resonance region (Au, Co, Na, and W) are characterized by the fact that the main contribution to their resonance activation integrals are made by the first lower resonance and $1/v$ cross section. Ignoring the contribution of higher resonances made it possible to analytically determine the parameters of the exponential function (1) in this region (exponential function was selected a priori based on physical considerations presented above) in a rather simple way. The parameter-determination algorithm was similar to the one for fast neutrons, but the isotope activity due to capture in the resonance region rescaled for infinite continuous irradiation time and one atom with energy dependence of the neutron flux expressed by (1) was calculated differently:

$$A_{\text{pac},i} = C_i(\beta) \times \left[\frac{0.707\sigma_0}{(\beta - 0.5)} \times 10^{6\beta - 1} + E_{\text{res}}^{1-\beta}(I_{\text{res}} - I_{1/v})\right]. \quad (5)$$

Here, the first item in brackets is the contribution of the capture reaction under $1/v$ law into the isotope activity in the energy region of 0.5 eV–0.5 MeV for the neutron-flux energy distributed under the power law (1), σ_0 is the cross section for 1 eV, the second item is the contribution of the neutron capture at the first resonance with energy E_{res} measured in eV into the isotope activity, I_{res} is the tabulated resonance integral for the Fermi spectrum, and $I_{1/v}$ is the contribution of $1/v$ to the resonance integral over the energy region of 0.5 eV–0.5 MeV for the Fermi distribution of neutron-flux energy ($\sqrt{2}\sigma_0$).

Values of C and β parameters for the flux funxtion (1) were reconstructed analytically using the same algorithm as the one used for $E > 5$ MeV. The illustrative example of $C_i(\beta)$ curves is presented at the plot in Fig. 6 for Au, Co, and Na isotopes. Values of C and β parameters of the exponential function (1) for the neutron flux at the distance of 0.3 m from the reactor moderator turned out to be as follows:

$$C_x = 0.39 \times 10^{12} \text{ n cm}^{-2} \text{ s}^{-1} \text{ MeV}^{-1}, \quad \beta_x = 0.88 \quad (6)$$

with an error of, at most, ±5% for the parameter C_x under the fixed β_x. The parameter C_x for the differential energy density of the neutron flux at a distance of 0.5 m turned out to be 2.17 times as small, whereas the exponent β_x remained the same.

In addition to the data presented above, the thermal neutron-flux density (for $E < 0.25$ eV) was obtained using the standard cadmium difference method. The value for gold (6.9×10^{11} n cm^{-2} s^{-1}) turned out to be higher than that measured for Cu^{63}, specifically, 6.76×10^{11} n cm^{-2} s^{-1}, by 2%. This discrepancy is explained by the effect of epithermal neutrons (0.25–0.5 eV) being taken into account with insufficient accuracy: the proximity of gold resonance (5 eV) leads to an overestimtion of the cadmium difference. The true flux density value is actually closer to the one measured for Cu.

It is worth noting that the presented errors are estimated under the assumption of absolute accuracy of the neutron data. The neutron cross sections used were taken from the evaluated neutron data file ENDF-B/VII, apart from those for indium and tin, whose cross sections of isomer formation were taken from the TENDL database [3]. The data from the JENDL database were used during processing as well, but the errors in the results turned out to be significantly higher in this case.

General Formula for the Flux in the Energy Region of 0.5 eV to 14 MeV

Thus, the shape of the differential neutron-flux density was reconstructed for $E > 1$ MeV and $E < 0.1$ MeV with a gap between them. A single common function for differential energy density of the neutron flux in the beam line no. 3 of the IBR-2 reactor may be used in actual calculations throughout the whole energy range from 0.5 eV to 14 MeV. This function covers the energy interval not covered by NAA and has smooth transitions into the function of resonance neutron flux on

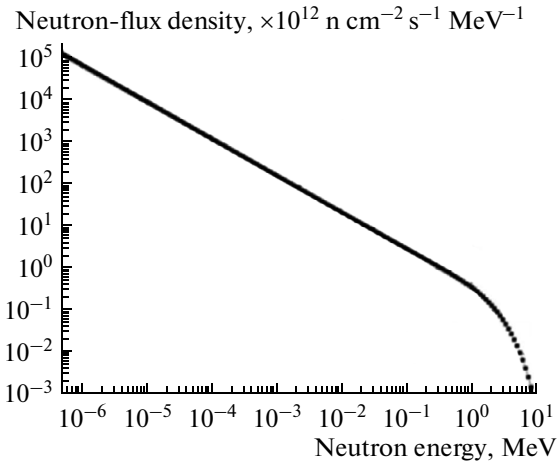

Fig. 7. Differential neutron-flux density in the beam line no. 3 of the IBR-2 reactor at the distance of 0.3 m from the reactor moderator (the NAA results with artificial filling of the energy range of 0.1–1 MeV).

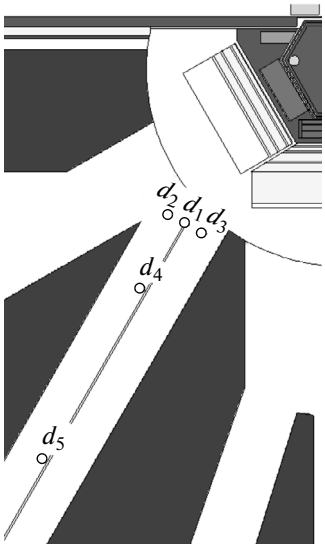

Fig. 8. Calculation geometry at a level of 6 m (beam axis plane) with an indication of points where neutron-flux density is calculated.

the left and into the function of fast neutron flux with energies $E > 1$ MeV on the right. It is written as follows:

$$\Phi(E) = \left(C_1 \cdot e^{-0.693E} + C_2 \cdot \frac{e^{-0.97E}}{E^{0.88}}\right) \times 10^{12} \text{ n cm}^{-2} \text{ s}^{-1} \text{ MeV}^{-1}. \quad (7)$$

In fact, exponential terms in the resonance region rapidly tend to one as energy decreases, the relation of the first item to the second one tends to zero (it already equals 0.02 at $E = 0.01$ MeV), and function (7) acquires form (1). The second item of both (4) and (7) in the high-energy region of $E > 3$ MeV is negligible in comparison with the first one, whereas the function values in the energy region of 1 MeV $< E <$ 3 MeV differ by less than 2%. The C coefficients only depend on the distance to the reactor moderator L (restricted to 0.3–0.7 m) and are presented in the table below.

The NAA approximation of differential energy density of the neutron flux in the beam line no. 3 of the IBR-2 reactor at a distance of 0.3 m from the reactor moderator calculated using the unified formula (7) is presented in Fig. 7.

4. COMPARISON WITH THE CALCULATED SPECTRUM

The differential energy density of the neutron flux in the beam line no. 3 of the IBR-2 reactor was calculated at several points corresponding to locations of the activated samples (Fig. 8).

The calculation was performed using the 3D MCNP-X5 model with the ENDF/B-VII cross-section library [4] for geometry and composition of materials as closely matched to the reactor specification requirements as possible. The output data were presented using the multigroup approximation (23 groups for each energy decade, which are uniformly distributed over the lethargy, i.e., energy logarithm) and normalized by one fission neutron in the active core of the reactor.

A comparison of the calculated fluxes and the ones reconstructed using NAA (for the reactor power of 1.86 MW, i.e., the power at which isotopes were irradiated) is presented at plots in Figs. 9 and 10. Significant differences may be observed in both fast neutron region with $E > 0.1$ MeV (experimental values are lower than the calculated ones) and resonance and

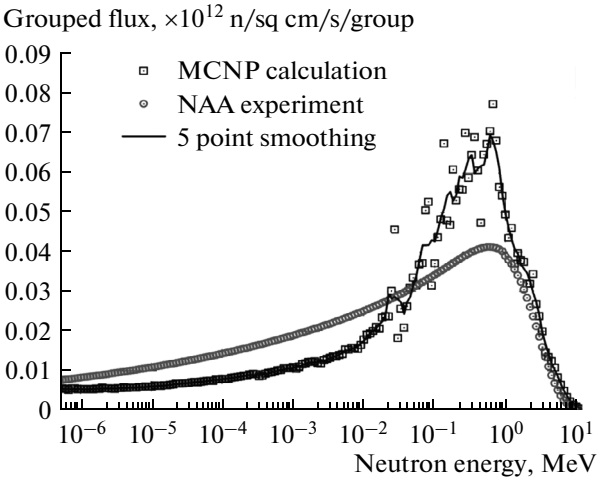

Fig. 9. Grouped neutron fluxes obtained via calculation (squares and the approximmating curve) and experimental NAA reconstruction (circles).

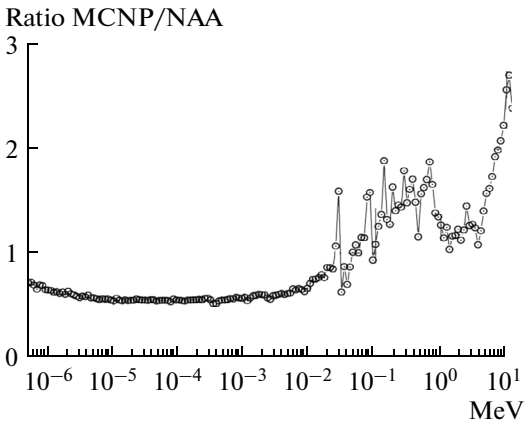

Fig. 10. Relation of the calculated flux to the one measured using NAA (based on Fig. 9).

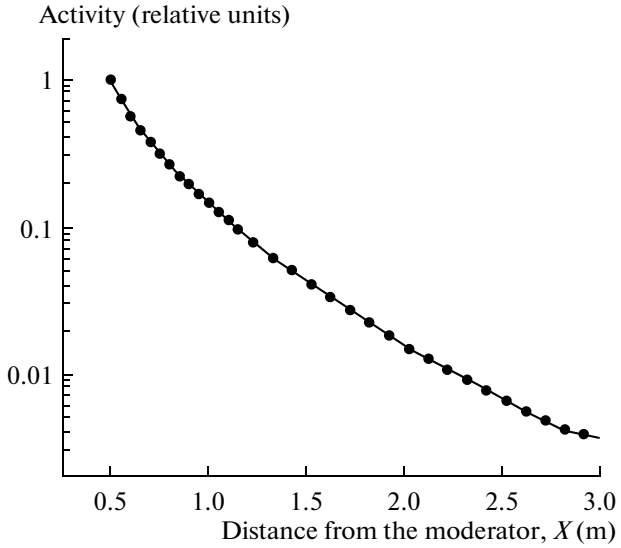

Fig. 11. Induced activity distribution for Ni along the beam.

thermal neutron region, where the opposite pattern is observed. Here, the difference in the integrated flux is less than 10%. It should be remembered that it was not possible to reconstruct the spectrum shape in the neutron energy range of 0.1–1 MeV using NAA.

The calculated thermal neutron-flux density turned out to be ~80% of the one reconstructed using NAA for copper.

The result that was obtained cannot be explained by any kind of systematic errors of the spectrum reconstruction algorithm, since the isotope activity directly calculated based on the MCNP data is significantly higher than the experimentally measured activity (Table 2). The harder neutron spectrum obtained using the MCNP software has not been explained yet. The causes of discrepancy between the calculation and the experiment will be found in future investigations.

A comparison with the results of previous NAA measurements of spectral density of neutron fluxes in the vicinity the moderator surface ([5]) would be of interest. Taking into account the measurement location correction (according to the calculation, flux densities in the vicinity of the moderator are 2.5 times as high as the ones at the distance of 300 mm), the results of both investigations are comparable in the thermal neutron region and in the fast neutron region with energies of 0.1–3 MeV, whereas the previous data

Table 2. Threshold reaction rates for fast neutrons (A_∞, reactions/s/atom of the initial isotope) obtained experimentally and calculated based on the reconstructed spectrum and the calculated spectrum

Reaction	Experiment, 0.3 m from the reactor	Experiment, 0.5 m from the reactor	MCNP calculation for 0.3 m	Calculation based on NAA spectrum for 0.3 m	Relative deviation from the experiment (columns 2 and 5)
V-51(n, α) Sc-48	9.4E-18	4.35E-18	1.76E-17	9.7E-18	+0.031
Al 27(n, α) Na-24	3.1E-16	1.6E-16	6.0E-16	3.1E-16	0
Ti-46(n, p) Sc-46	4.75E-15	2.19E-15	6.18E-15	4.56E-15	–0.04
Ti-47(n, p) Sc-47	7.3E-15	3.28E-15	9.9E-15	8.0E-15	+0.095
Ti-48(n, p) Sc-48	1.36E-16	6.28E-17	1.96E-16	1.42E-17	+0.04
Fe-54((n, p) Mn-54	3.39E-14	1.56E-14	5.52E-14	3.4E-14	0.003
Ni-58((n, p) Co-58	4.6E-14	2.11E-14	7.87E-14	4.5E-14	–0.021
In-115(n, n') In-115m	10.6E-14	–	–	10.6E-14	0
Sn-117(n, n') Sn117m	1.32E-14	0.61E-14	–	1.33E-14	+0.008

are significantly smaller, i.e., 1.5 times as small, for higher energies.

5. SPATIAL DISTRIBUTION PATTERN OF NEUTRON-FLUX DENSITY

The neutron spectrum was also measured at a distance of 3.125 m from the reactor moderator (at the far end of the supporting beam). The spectrum is significantly harder at this distance: the flux becomes 40 times as weak as the one at the distance of 0.5 m at energies above 5 MeV and about 100 times as weak at medium energies of 1–5 MeV; the thermal neutron flux becomes 170 times as weak.

An induced activity distribution was measured for Ni *continuously along the whole beam length* (see Fig. 11). Flux intensity distribution at 0.3–1 m from the reactor approximately follows an exponential law with a twofold reduction at a length of 18 cm. In other words, the flux gradient is about 4% per 1 cm.

Significant gradients of 2%/cm in average for a length of 10 cm take place *in the lateral cross section of the beam line* in the supporting beam area. The flux decreases from left to right if the line of sight is directed along the beam direction towards the reactor. The lateral gradient is related to peculiarities of the reactor shield geometry (Figs. 1, 8). It should be taken into consideration when choosing sample placement and sizes. In the case of large-scale samples, gradients may be reduced via the installation of neutron reflectors; however, this procedure requires long preparations.

ACKNOWLEDGMENTS

We thank S.S. Pavlov (Neutron Physics Laboratory of the Joint Institute for Nuclear Research) for providing the set of reference radiation sources for a long period of time and Yu.P. Kharitonov (Institute in Physical and Technical Problems) for invaluable help in mastering the operation of the gamma spectrometer.

REFERENCES

1. Nuclear Physics in the Internet, Activation Analysis. http://nuclphys.sinp.msu.ru/nuc_techn/activ_analy.htm
2. X-5 Monte Carlo Team, "MCNP—A General Monte Carlo Transport Code, Version 5," Los Alamos National Laboratory Report LA-UR-03-1987, Los Alamos National Laboratory (2003).
3. TENDL-2013: TALYS-Based Evaluated Nuclear Data Library. ftp://ftp.nrg.eu/pub/www/talys/tendl2013/tendl2013.html
4. "ENDF/B-VII.1 Nuclear Data for Science and Technology: Cross Sections, Covariances, Fission Product Yields and Decay Data," Nucl. Data Sheets **112** (12), 2887–2996 (2011); Unclassified Report LA-UR 11-05121, Los Alamos National Laboratory.
5. V. V. Golikov, E. N. Kulagin, and E. P. Shabalin, "Dose Rates near the Water Moderator of the IBR-2 Reactor: Experiment and Analysis," Preprint No. E16-2002-79, OIYaI (Joint Institute for Nuclear Research, Dubna, 2002).

Translated by A. Amitin